Drastic changes in a lower-trophic-level ecosystem attributed to unprecedented harmful algal outbreaks in 2021 on the Pacific shelf off southeast Hokkaido, Japan

Continental Shelf Research 267 (2023) 105114

Contents lists available at ScienceDirect

Continental Shelf Research

journal homepage: www.elsevier.com/locate/csr

Drastic changes in a lower-trophic-level ecosystem attributed to unprecedented harmful algal outbreaks in 2021 on the Pacific shelf off southeast Hokkaido, Japan

Yukiko Taniuchi [a], Tsuyoshi Watanabe [a], Tomonori Azumaya [a], Satomi Takagi [a], Hiromi Kasai [a], Takuya Nakanowatari [a], Takuya Ohnishi [a], Shigeho Kakehi [b], Hiroshi Kuroda [a,*]

[a] Fisheries Resources Institute (Kushiro Station), Japan Fisheries Research and Education Agency, 116 Katsurakoi, Kushiro, Hokkaido, 085-0802, Japan
[b] Fisheries Resources Institute (Shiogama Station), Japan Fisheries Research and Education Agency, 3-27-5 Shinhama-cho, Shiogama, Miyagi, 985-0001, Japan

ARTICLE INFO

Keywords:
Harmful algal bloom
Karenia selliformis
Phytoplankton community
Nutrients

ABSTRACT

Unprecedented, large-scale harmful algal blooms (HABs) occurred in Pacific coastal shelf waters off the southeastern coast of Hokkaido, Japan, in the autumn of 2021. To understand how these HABs, composed primarily of *Karenia selliformis*, changed the structures of lower-trophic-level ecosystems in shelf waters, we analyzed high-resolution *in situ* ship measurements taken during October 2015–2021. We mainly compared physico-biochemical variables averaged over the shelf in 2021 and in 2015–2020. Chlorophyll-*a* concentrations at a depth of 10 m were approximately 2.3-fold higher in 2021 than in 2015–2020. Chlorophyll-*a* concentrations were highest at the sea surface in 2021, and vertically integrated concentrations were 1.8-fold higher in 2021 than in 2015–2020. Silicate concentrations at a depth of 10 m were higher in 2021, whereas nitrate and phosphate concentrations were largely the same. Abundances of major diatoms and picophytoplankton (e.g., *Synechococcus* spp.) at a depth of 10 m declined by 2 orders and 1 order of magnitude in 2021, respectively, whereas *Karenia* spp. abundance greatly increased. These results indicated that outbreaks of *K. selliformis* suppressed the growth of other algal species and dramatically changed nutrient flows and balances in the coastal shelf ecosystem. The suppression of non-*Karenia* algal species might have occurred through interspecific competition for nutrients as well as allelopathy and/or mixotrophy by *K. selliformis*.

1. Introduction

Harmful algal blooms (HABs) are a critical global problem. Their increasing frequency and severity and expanding niche can be related to climate change (e.g., Frölicher and Laufkötter, 2018; Gobler et al., 2017; Gobler, 2020; IPCC, 2019; Trainer et al., 2019; Wells et al., 2015, 2020). Large-scale HABs can inflict devastating damage on marine ecosystems and human wellbeing, and since the 1990s, most have been accompanied by basin-scale marine heatwaves (MHWs) (Hobday et al., 2016) associated with anomalously high temperatures (Bondur et al., 2021; Lefebvre et al., 2016; McCabe et al., 2016; Roberts et al., 2019; Ryan et al., 2017; Smith et al., 2021). In fact, the global count of MHW days per year has risen over the historical record because of increases in the duration and frequency of MHWs (Oliver et al., 2018). This trend is projected to increase further under climate change because of long-term ocean warming (Frölicher et al., 2018; Oliver et al., 2019, 2021). Further increases of damage from HABs are therefore an urgent concern for the future.

In mid-September 2021, unprecedented large-scale HABs (hereafter referred to as the "2021 HABs") occurred in Pacific coastal shelf waters off the southeastern coast of Hokkaido, Japan (Hasegawa et al., 2022; Kuroda et al., 2021a; Yamaguchi et al., 2022) about a month after the subsidence of an MHW of record-breaking extent and intensity over the northwestern Pacific Ocean (Kuroda and Setou, 2021). The 2021 HABs were characterized by their large spatial scale (>300 km in the alongshore direction) and prolonged duration (several months) (Kuroda et al., 2022). Previously, there had been no reports of large-scale HABs over the entirety of this study region, where the marine environment has remained largely in a natural, healthy condition. Ocean circulation was not unusual around Pacific coastal shelf waters at the beginning of the 2021 HABs (Kuroda et al., 2021a), except for a stable, persistent front among subtropical and subarctic waters in the downstream area of the

* Corresponding author.
E-mail addresses: kurocan@affrc.go.jp, kuroda_hiroshi23@fra.go.jp (H. Kuroda).

https://doi.org/10.1016/j.csr.2023.105114
Received 23 May 2023; Received in revised form 22 August 2023; Accepted 4 September 2023
Available online 6 September 2023

HABs (Higashi and Nakada, 2022). Kuroda et al. (2021a) have suggested that the generation of the 2021 HABs was fueled by the vertical entrainment of oceanic nutrients caused by intermittent and seasonal deepening of mixed layers after mid-August, when the MHWs subsided abruptly. The 2021 HABs were predominantly composed of *Karenia selliformis, K. mikimotoi, K. longicanalis*, and other dinoflagellates (Iwataki et al., 2022). *K. selliformis* is an alien species in Japanese waters that was first found in great abundance in this region during the 2021 HABs. Particle-tracking experiments (Kuroda et al., 2021a) and rDNA sequence analysis (Iwataki et al., 2022) have suggested that *K. selliformis* could have been transported to the area from the east coast of the Kamchatka Peninsula, which also experienced unprecedented outbreaks of mainly *K. selliformis* in the autumn of 2020 (Orlova et al., 2022), just a year prior to the 2021 HABs.

Serious damages caused by the 2021 HABs to coastal fisheries were reported off southeast Hokkaido. For example, in areas of the Pacific shelf along the southeast Hokkaido coast, where massive blooms of *Karenia* spp. occurred (Fig. 1A), sea urchins experienced mass die-offs, adult chum salmon, *Oncorhynchus keta*, died in fixed nets, and juvenile fish died in rearing facilities. According to Hokkaido prefecture, the total economic damage to coastal fisheries as of February 16, 2023 was about 70 million US dollars (at an exchange rate of 130 Japanese yen to 1 US dollar), which is the highest cost incurred by Japanese fisheries in the historical record. After the 2021 HABs, Hokkaido prefecture commissioned submersible surveys to identify the distribution and extent of damage to commercial fish species around Pacific coastal shelf waters. However, few studies have examined the effects of the 2021 HABs on non-commercial species, including the lower-trophic-level ecosystem, which is fundamental to the marine food web. In fact, numerical simulations based on a lower-trophic-level ecosystem model (Takagi et al., 2022) have suggested that the appearance of *K. selliformis* in the 2021 HABs drastically changed lower-trophic-level ecosystem structures in shelf waters in terms of nutrient flows and balances. However, most of the changes detected in this numerical simulation have not been verified by comparison to *in situ* data. Informed understanding of the effects of the 2021 HABs on the lower-trophic-level ecosystem therefore first requires a comparison of regular *in situ* monitoring data collected during 2021 with data collected during other years.

In terms of broad oceanographic conditions, the 2021 HABs appeared primarily at the sea surface in Pacific coastal shelf waters near the confluence of the Oyashio and Coastal Oyashio currents (Fig. 1B; Kuroda et al., 2022). The Oyashio, which is the western boundary current of the North Pacific western subarctic gyre (Kuroda et al., 2021b), transports subarctic, nutrient-rich water along a slope region associated with high productivity (e.g., Sakurai, 2007). The Coastal Oyashio, which is located inshore of the Oyashio, flows westward along the Pacific shelf as a coastal boundary current throughout the year and transports mixed waters known as Modified Soya Warm Current Water during summer–autumn. This water originates in the Sea of Japan in a subtropical water mass known as the Tsushima Warm Current Water, which is then modified by mixing with ambient subarctic waters during its transport via the Sea of Okhotsk to the Pacific shelf by the Soya Warm Current (Fig. 1B). To monitor Oyashio and Coastal Oyashio conditions, the Japan Fisheries Research and Education Agency has regularly conducted *in situ* measurements of the lower-trophic-level ecosystem along the A Line (near the Oyashio) since 1987 (e.g., Kuroda et al., 2017; Saito et al., 1998) and along the L lines (in Pacific coastal shelf waters) since 2015 (e.g., Kuroda and Toya, 2020; Kuroda et al., 2021c) (Fig. 1B). The core of *Karenia* outbreaks in October 2021 was successfully documented by the L line surveys (Fig. 1).

The main purpose of this study was to understand how the 2021 HABs affected the lower-trophic-level ecosystem in coastal shelf waters with a special focus on phytoplankton community structure and nutrients. We further emphasize that the primary focus of this study was not limited to a specific water mass with patchy outbreaks of *Karenia* spp. Instead, this study averaged overall conditions over the Pacific shelf off southeast Hokkaido during the 2021 HABs. To do so, we mainly used the regular *in situ* monitoring data collected along the L lines to compare environmental conditions between 2021 and 2015–2020.

2. Materials and methods

2.1. High-resolution in situ measurements along the L lines

We performed high-resolution ship surveys during October 2015–2021 in shelf waters off the southeastern Pacific coast of Hokkaido (Fig. 1B) from aboard the research vessel R/V *Hokko-maru*. Conductivity–temperature–depth (CTD) measurements along across-shelf transects were conducted on the L lines (i.e., L1–L7). Measurement stations were placed at intervals of about 2 km to capture submesoscale

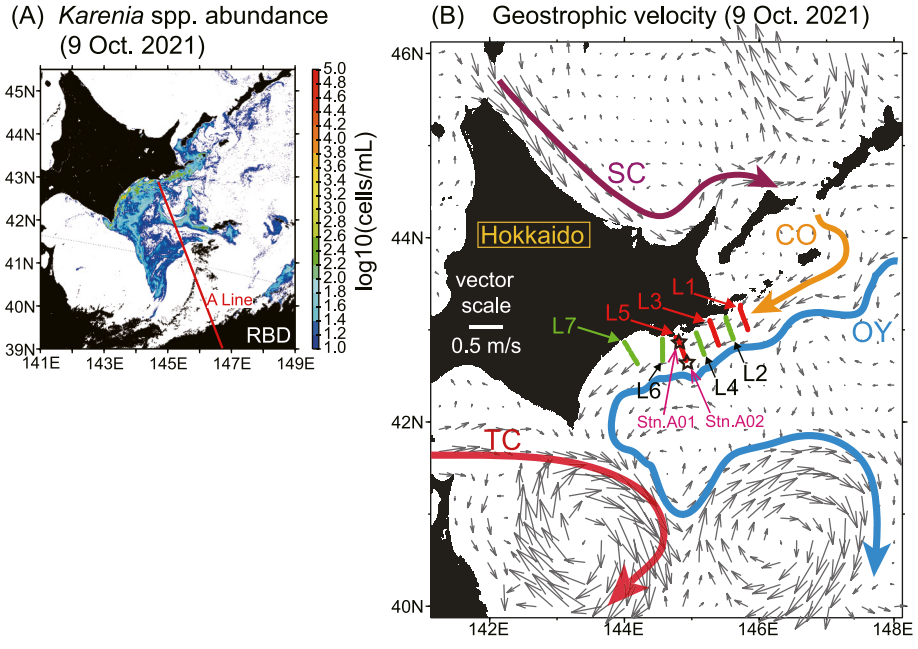

Fig. 1. (A) Map of *Karenia* spp. abundance on October 9, 2021 as estimated from the red-band difference (RBD) of Sentinel-3 data. The position of the A Line is shown by the red line. (B) Map of absolute geostrophic velocity at the sea surface (grey vectors) based on altimetry data on October 9, 2021. Schematic representations of ocean currents are depicted by thick arrows. SC, Soya Warm Current; CO, Coastal Oyashio; OY, Oyashio; TC, Tsugaru Warm Current. Red lines show the L lines analyzed in this study (i.e., L1, L3, and L5), and green lines show the L lines not analyzed in this study. Open stars show Stations A01 and A02.

variability on the shelf. Table S1 and Fig. S1 provide detailed information about each station. We used a Sea-Bird Electronics (SBE) 911plus CTD system (Sea-Bird Electronics, Inc., WA, USA) for all surveys except the 2017 survey, when we used a SBE 19plus CTD system. In 2018, we used an expendable conductivity–temperature–depth system (XCTD-1; Tsurumi Seiki, Co. Ltd., Tokyo, Japan) at some stations instead of a CTD system. An optical sensor to measure fluorescence and turbidity (ECO FLNTURTD; WET Labs, OR, USA) and a dissolved oxygen sensor (SBE43; Sea-Bird Electronics, Inc.) were attached to the CTD sensor. These sensors together with the CTD sensor were lowered to the vicinity of the seafloor or to a depth of 490 m. For surveys conducted in 2015, we independently lowered a water quality profiler (AAQ1183; JFE Advantech Co. Ltd., Hyogo, Japan) to a depth of 100 m instead of attaching additional sensors to the CTD sensors.

At all CTD stations, temperature, salinity, nutrient concentrations (i.e., nitrate, nitrite, silicate, and phosphate), chlorophyll-*a* concentrations, and rarely abundance of diatoms and dinoflagellates were measured in sea surface water sampled with a bucket. Water at standard depths (10, 20, 30, 50, 75, 100, 150, 200, 300, 400, and 490 m) was sampled via Niskin bottles on a CTD-rosette sampler system. The water sampled from the L lines was aliquoted into smaller bottles on deck for transport to a shore-based laboratory, where we measured salinity/conductivity (200 or 250 mL at the sea surface), nutrient concentrations (10 mL × 4 subsamples at the sea surface and all standard depths), chlorophyll-*a* concentrations (100 mL at the sea surface), abundance of diatoms and dinoflagellates (500 or 1000 mL normally at depths of 0 m and 10 m mostly in 2017 and 2018), and abundance of picophytoplankton (1.5 mL × 2 subsamples at a depth of 10 m in only 2020 and 2021). Water samples for estimates of phytoplankton abundance were collected only from L1, L3, and L5 every other station (i.e., 4-km intervals). Water samples for enumeration of diatoms and dinoflagellates that were collected at the sea surface in 2017 and 2018 were also used to confirm the absence of *Karenia* spp.

2.2. Sensor-value correction by using in situ measurements along the A line

In situ measurements at Stations A01–A21 and B01–B04 along the A Line (Fig. 1A) were used to correct vertical profiles of CTD-based sensor values (i.e., salinity/conductivity and fluorescence) along the L lines. Table S2 and Fig. S2 provide detailed information about each station. For each cruise in October during 2015–2021, *in situ* measurements were carried out along the A Line before the L line measurements. A CTD with optical and dissolved oxygen sensors was lowered to the vicinity of the seafloor or to a depth of 3100 m, whichever was reached first, at stations along the A Line. Waters at standard depths (10, 20, 30, 40, 50, 60, 80, 100, 125, 150, 200, 300, 400, 500, 600, 800, 1000, 1250, 1500, 2000, 2500, and 3000 m) were sampled by using Niskin bottles on a CTD–rosette sampler system. We obtained water samples for measurements of conductivity/salinity (200 mL at standard depths) and chlorophyll-*a* concentration (100 mL at standard depths above 200 m).

For each cruise, sensor values were plotted against corresponding values determined by analytical measurements made manually on water samples at shore-based facilities (see section 2.3) to obtain a regression line. The regression line was then used to correct profiles of salinity and chlorophyll-*a* concentrations along the L lines. The R^2 values of the regression lines were 0.9988–0.9998 for salinity and 0.561–0.974 for chlorophyll-*a* concentrations. Details and scatter plots regarding the correction of chlorophyll-*a* concentrations are shown in Fig. S3. Profiles of corrected sensor values were analyzed for depths >5 m.

2.3. On-board preprocessing and shore-based measurements

Salinity/conductivity, chlorophyll-*a* concentrations, nutrient concentrations, and abundances of phytoplankton (i.e., diatoms, dinoflagellates, and picophytoplankton) were measured using the aliquoted water samples collected from the A Line and L lines in a shore-based laboratory at the Fisheries Resources Institute (Kushiro Station).

Salinity/conductivity was measured with high accuracy with a Model 8400B "Autosal" Laboratory Salinometer (Guildline Instruments, ON, Canada).

Chlorophyll-*a* concentrations were measured manually via the procedures described by Kasai et al. (1998). Water samples were filtered onto 25-mm Whatman GF/F glass fiber filters immediately after sampling and preserved in N,N-dimethylformamide as described by Suzuki and Ishimaru (1990). Samples and filters were frozen onboard the R/V *Hokko-maru* and stored in the dark until they could be measured with a fluorometer (Model 10AU; Turner Designs, CA, USA) at a shore-based laboratory.

Nutrient samples were collected in acrylic disposable tubes and immediately frozen on board until measurement at a shore-based laboratory. Concentrations of nitrate, nitrite, silicate, and phosphate were measured with an autoanalyzer (AACS-III; Bran + Luebbe, Norderstedt, Germany) following the methods described by Strickland and Parsons (1972) and Oguma et al. (2008).

For enumeration of diatoms and dinoflagellates, water samples of 500–1000 mL were fixed with acid Lugol's solution (final concentration, 4%) and preserved at 5 °C on board. At a shore-based laboratory, water samples for enumeration of diatoms and dinoflagellates were concentrated to a volume of 25–50 mL by reverse filtration through 2-μm pore-size filters (Dodson and Thomas, 1964). Phytoplankton (>5 μm) in the concentrated samples were identified and counted under a light microscope. Identification of diatom and dinoflagellate species and their main habitats was based on information in Hasle and Syvertsen (1997). *Karenia* spp. were taxonomically identified based on the results of Iwataki et al. (2022).

Picophytoplankton were counted on a laser-equipped flow cytometer (excitation frequency 488 nm, standard filter set, NovoCyte 2070V; Agilent, CA, USA) following the protocol described by Suzuki et al. (2005). Water samples of 1.5 mL were fixed with paraformaldehyde (final concentration, 0.2%) for 5–10 min and frozen in liquid nitrogen. After the cruise, samples were kept at −80 °C until analysis. Analyses were made on duplicate samples. Each thawed sample was passed through a 35-μm cell strainer (Beckman Coulter, CA, USA) to remove large plankton and detritus. To quantify cell sizes, 2-μm beads of Fluoresbrite YG Microspheres (Polysciences, PA, USA) were mixed into the samples. Cells that contained chlorophyll-*a* and had no phycoerythrin were counted as picoeukaryotes. Cells that contained both chlorophyll-*a* and phycoerythrin and were less than 2 μm in size were counted as *Synechococcus*.

2.4. Statistical tests

Observed values were averaged during the period 2015–2020 over lines L1, L3, and L5, where the phytoplankton abundances were monitored, and compared against averaged values from 2021. We applied Welch's *t*-test to identify significant differences of the mean values of a specific environmental variable (e.g., temperature, salinity, phosphate concentration, chlorophyll-*a* concentration) between the two time periods. The advantage of this test was that it does not require homoscedasticity, an assumption that was not satisfied for many of the variables we analyzed (data not shown). $P \leq 0.05$ was employed as the threshold for significance.

3. Results

3.1. Differences of each environmental variable at a depth of 10 m between 2015–2020 and 2021

Prior to comparing the spatial distribution of each environmental variable at a depth of 10 m between October 2015–2020 and 2021, we examined year-to-year changes in the distribution of *Karenia* spp.

abundance at depths of 0 m or 10 m in October 2015–2021 (Fig. 2). *Karenia* spp. were not identified in October 2015–2019, were identified at very low abundances ($<2.62 \times 10^2$ cells L^{-1}) at some stations along the L1, L3, and L5 lines in 2020, and were identified at higher abundances (2.33×10^3 to 2.77×10^5 cells L^{-1}) at all sampling stations along the same three lines in 2021. The spatial distribution of *in situ Karenia* spp. abundance in 2021 was qualitatively consistent with satellite-derived *Karenia* spp. abundances (Fig. 1A). Particularly high abundances were patchily distributed at stations L5-03 (1.67×10^5 cells L^{-1}), L5-09 (9.77×10^4 cells L^{-1}), and L5-11 (2.77×10^5 cells L^{-1}) along the L5 Line (Fig. 2). The distance of ~4 km between adjacent sampling stations appeared to be too large to accurately capture the continuous distribution of *Karenia* spp. abundance because the width of streak-like filaments of high *Karenia* spp. abundance at the sea surface was typically a few kilometers according to the *in situ* and satellite-based analyses of Kuroda et al. (2022).

We compared the spatial distribution of each variable at a depth of 10 m along L1, L3, and L5 between October 2015–2020 (i.e., 6-year averages) and 2021 (Figs. 3–5). Year-to-year distributions of each environmental variable at a depth of 10 m are summarized in Fig. S4. Overall, temperatures at a depth of 10 m were lower in 2021 than in 2015–2020 (Fig. 3A). Salinities at a depth of 10 m were higher and more horizontally homogeneous in 2021 (Fig. 3B). Temperatures (12.3–14.5 °C) and salinities (33.23–33.54) at a depth of 10 m in 2021 largely corresponded to Modified Soya Warm Current Water (generally defined by temperatures >7.0 °C and salinities of 33.0–33.7 on the Pacific shelf off southeastern Hokkaido; Kusaka et al., 2013). Chlorophyll-*a* concentrations (Fig. 3C) tended to be higher in 2021, and particularly high chlorophyll-*a* concentrations (>10 mg m^{-3}) were observed in the middle sections of L5, where *Karenia* spp. abundance exceeded 9.77×10^4 cells L^{-1}. This pattern was consistent with results reported by Kuroda et al. (2022) that revealed a positive correlation between chlorophyll-*a* concentrations and the abundances of *Karenia* spp. across a nearshore-to-offshore transect in October 2021. Mixed layer depths[1] varied considerably among stations in both 2015–2020 and 2021, and they differed considerably at each station between the two periods (Fig. 3D).

Nitrate concentrations averaged during 2015–2020 (1.16–2.80 μM) were relatively constant among stations but tended to increase slightly in the offshore direction, particularly along L1 and L3 (Fig. 4A). Nitrate concentrations in 2021 (0.10–5.40 μM) were considerably more variable; concentrations along L5 (0.10–1.90 μM) were extremely low, and those along L1 and L3 (1.30–5.40 μM) increased in the offshore direction more strongly than during 2015–2020. Phosphate and silicate concentrations in 2021 (Fig. 4B and C) varied less among stations than did nitrate concentrations (Fig. 4A). Phosphate concentrations tended to be slightly higher in 2021 than in 2015–2020, and silicate concentrations were much higher in 2021 than in 2015–2020. The resemblance between the spatial patterns of N/P and N/Si ratios in 2021 (Fig. 4D and E) to that of nitrate concentrations (Fig. 4A) implies that the N/P and N/Si ratios in 2021 were determined mainly by nitrate concentrations. The N/P and N/Si ratios during 2015–2020 increased in the offshore direction because nitrate concentrations during 2015–2020 tended to increase in the offshore direction, and phosphate and silicate concentrations tended to decrease in the offshore direction along each L line.

Abundances of the four categorized phytoplankton groups (i.e., diatoms, dinoflagellates, picoeukaryotes, and *Synechococcus* spp.) were lower in 2021 than in 2015–2020 (Fig. 5). Note that there was sampling bias because of missing measurements of phytoplankton samples at a depth of 10 m, as discussed in sections 4.2 and 4.3, and the abundances of picoeukaryotes and *Synechococcus* spp. at a depth of 10 m were obtained only in 2020 and 2021 (see Figs. S4H–K). Abundances of diatoms in 2021 were extremely low along L5 (1.36×10^3 to 2.47×10^4 cells L^{-1}), where *K. selliformis* was the most abundant (Fig. 2). Abundances of dinoflagellates in 2021 were also similar to or lower than those during 2015–2020 along L1 and L3, but their higher abundance during 2021 than during 2015–2020 at most stations along L5 was associated with outbreaks of *K. selliformis*.

Next, to focus on average conditions over the targeted Pacific shelf, we used Welch's *t*-test to statistically compare environmental variables along the L1, L3, and L5 lines at a depth of 10 m between 2015–2020 and 2021. Temperatures were significantly lower in 2021 than in 2015–2020, and salinities were significantly higher in 2021 (Fig. 6A and B). The smaller variances for these two variables in 2021 than in 2015–2020 indicated that water masses at a depth of 10 m on the Pacific shelf were spatially nearly homogeneous in 2021. The variance of mixed layer depths was also smaller in 2021 than in 2015–2020, but mixed layer depths in 2021 were not significantly different from those in 2015–2020 (Fig. 6D). Chlorophyll-*a* concentrations in 2021 (mean, 4.398 mg m^{-3}) were approximately 2.3 times those in 2015–2020 (mean, 1.954 mg m^{-3}) (Fig. 6C). The minimum chlorophyll-*a* concentration in 2021 (0.888 mg m^{-3}) was higher than the 25th-percentile value for 2015–2020 (0.649 mg m^{-3}), and the maximum reached 20.135 mg m^{-3}.

Nitrate concentrations did not change very much between the two time periods, although the mean was slightly larger during 2021 (2.23 μM) than during 2015–2020 (1.78 μM). However, spatial averaging over the three L lines (Fig. 6E) masked the extremely low nitrate concentrations that appeared along L5 in 2021 (Fig. 4A). Phosphate concentrations were not significantly different during 2021 than 2015–2020 (Fig. 6F), but silicate concentrations were significantly higher in 2021 than in 2015–2020 (Fig. 6G). These results indicate that silicate was not a limiting nutrient at a depth of 10 m over the shelf in October 2021, and this excess silicate was associated with a low abundance of diatoms during that time (Fig. 5A).

Abundances of the 10 most-abundant dinoflagellate and diatom taxa (five single species and five multi-species groups) at a depth of 10 m during 2015–2021 were compared between 2021 and 2015–2020 together with other dinoflagellates and diatoms (Fig. 7 and Table 1). The sum of abundances of all 12 of these categorized taxa was 579,020 cells L^{-1} in 2015–2020 and 65,857 cells L^{-1} in 2021. There was hence a 8.8-fold reduction in abundance of these taxa between these two time periods.

Among dinoflagellates, the abundance of *Karenia* spp. increased dramatically in 2021 compared to 2015–2020 (Fig. 7A). *Ceratium kofoidii*, *Gonyaulax* spp., and *Scrippsiella* spp. also increased greatly (Fig. 7C–E) from very low levels in 2015–2020. In contrast, the abundance of *Gyrodinium* spp. less changed, and abundances of other dinoflagellates declined slightly from 345 to 224 cells L^{-1}. Hence, the abundance change of dinoflagellates was taxa dependent.

Diatom abundances declined significantly in 2021 relative to 2015–2020, with the exception of *Lauderia annulata*. Diatoms whose abundances declined by 2 orders of magnitude included *Skeletonema costatum* (from 362,244 to 4976 cells L^{-1}), *Thalassiosira* spp. (from 131,154 to 9970 cells L^{-1}), *Leptocylindrus danicus* (from 13,994 to 770 cells L^{-1}), *Asterionellopsis glacialis* (from 8407 to 476 cells L^{-1}), and other diatoms (from 60,901 to 1688 cells L^{-1}). Among picophytoplankton, *Synechococcus* spp. abundance declined drastically from 13,319 to 7575 cells L^{-1} (Fig. 6H).

The above results show that all the most abundant diatom taxa in 2015–2020 experienced drastic declines in abundance in 2021. Despite these declines, chlorophyll-*a* concentrations in 2021 increased significantly at a depth of 10 m. The indication is that the chlorophyll-*a* content per cell was higher in *Karenia* spp. than in major diatom taxa.

The relative abundances of the 12 categorized taxa differed greatly between 2015–2020 and 2021 (Fig. 8). *Skeletonema costatum* was the

[1] In this study, the mixed layer depth was estimated to be the depth at which the density in the upper layer exceeded a threshold value of 0.125 kg m^{-3} relative to the density at a depth of 10 m.

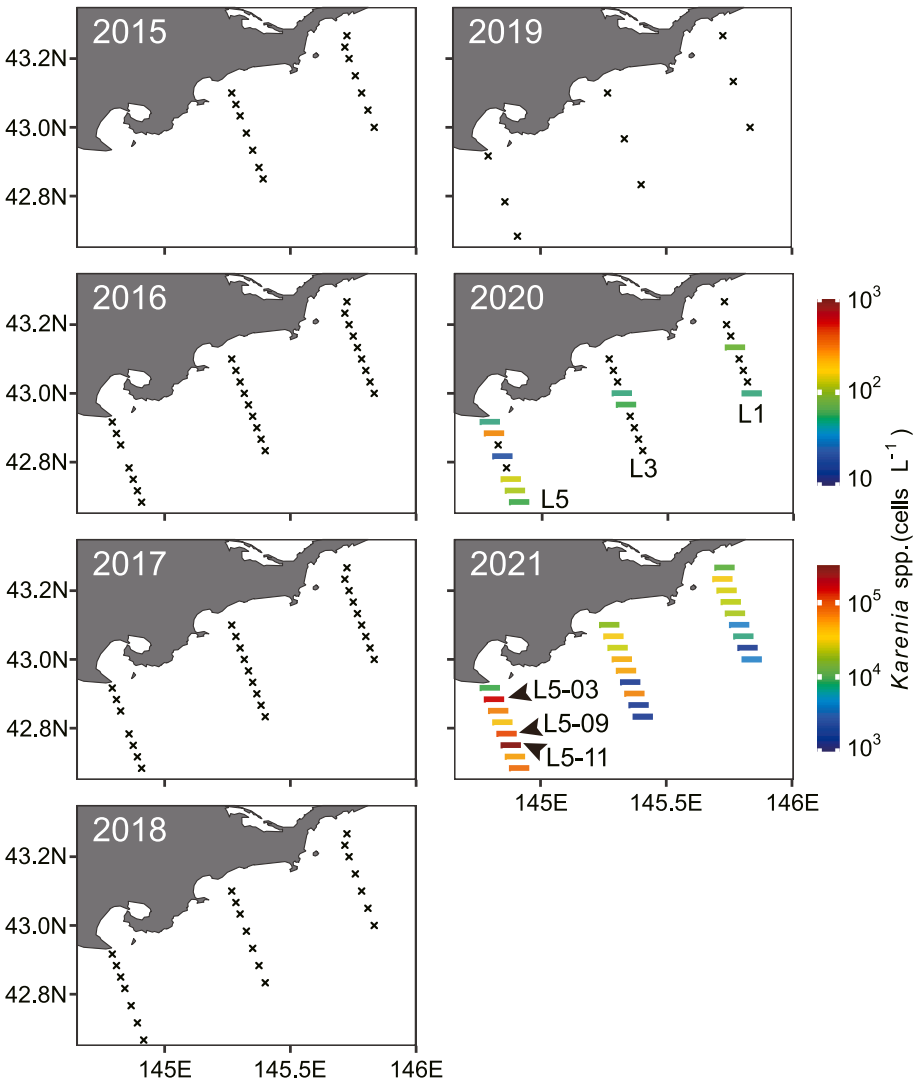

Fig. 2. *Karenia* spp. abundance near the sea surface (at 10-m depth, except in 2017 and 2018 when most measurements were at the sea surface) in October 2015–2021. Crosses indicate the absence of *Karenia* spp. Note that different scales of abundance are used for 2020 and 2021.

dominant species in 2015–2020 and accounted for 62.6% of the cells identified, but its abundance fell to 7.6% in 2021. The relative abundance of *Thalassiosira* spp. decreased moderately from 22.7% to 15.1%. Meanwhile, the relative abundance of *Karenia* spp. increased from <0.01% to 68.3%. These results suggest that outbreaks of *Karenia* spp. in autumn 2021 greatly reduced abundances of major diatoms and changed the composition of the predominant algal species.

3.2. Differences in vertical profiles between 2015–2020 and 2021

We compared vertical profiles averaged over the Pacific shelf and over the target period between 2015–2020 and 2021 (Fig. 9). Chlorophyll-*a* profiles clearly differed between the two periods (Fig. 9C). The difference was greatest at the sea surface, where concentrations in 2021 were 9.385 mg m^{-3}, 3.4 times the concentrations in 2015–2020 (2.725 mg m^{-3}). Kuroda et al. (2022) have reported that chlorophyll-*a* concentrations in 2021 were markedly increased at the sea surface. In other words, chlorophyll-*a* concentrations in 2021 decreased rapidly with depth in the upper 25 m and were almost comparable to those observed in 2015–2020 below a depth of 25 m. Because the average mixed layer depth in 2021 was 31 m (Fig. 6D), the sea surface–intensified chlorophyll-*a* concentrations in 2021, which were associated with a high abundance of *Karenia* spp., were limited to the interior of the mixed layer. Vertically integrated chlorophyll-*a* concentrations (from 0 to 200 m) were 1.8-fold higher in 2021 (155.9 mg m^{-2}) than in 2015–2020 (85.6 mg m^{-2}). The occurrence of *K. selliformis* therefore increased phytoplankton biomass in the water column overall.

Temperatures at depths of 0–200 m in 2021 ranged from 2.41 to 13.80 °C, and salinities ranged from 33.25 to 33.49 (Fig. 9A and B). The observed temperature and salinity profiles indicated the presence of Modified Soya Warm Current Water at depths of 0–100 m and Oyashio Water (generally defined by temperature ≤7 °C, salinity 33.0–33.7, and density <26.8 σ_θ; Kusaka et al., 2013) at depths of 100–200 m. A similar two-layer structure was observed in 2015–2020, but the contrast in salinity between the two layers was much clearer in 2021 and was characterized by a salinity maximum and minimum at depths of ~40 m and ~150 m, respectively. The higher nitrate, phosphate, and silicate concentrations across the entire studied depth range in 2021 versus 2015–2020 (Fig. 9D–F) indicates that the two water masses occupying coastal shelf waters originally contained higher concentrations of nutrients in 2021 than in 2015–2020.

Some deviations from this pattern, however, were apparent near the sea surface (here, 0–30 m). Nitrate and phosphate concentrations remained relatively unchanged between 2021 and 2015–2020 at shallow depths (i.e., at 0 and 10 m for nitrate and 10–30 m for phosphate). Similarly, N/P ratios were quite similar between the two time

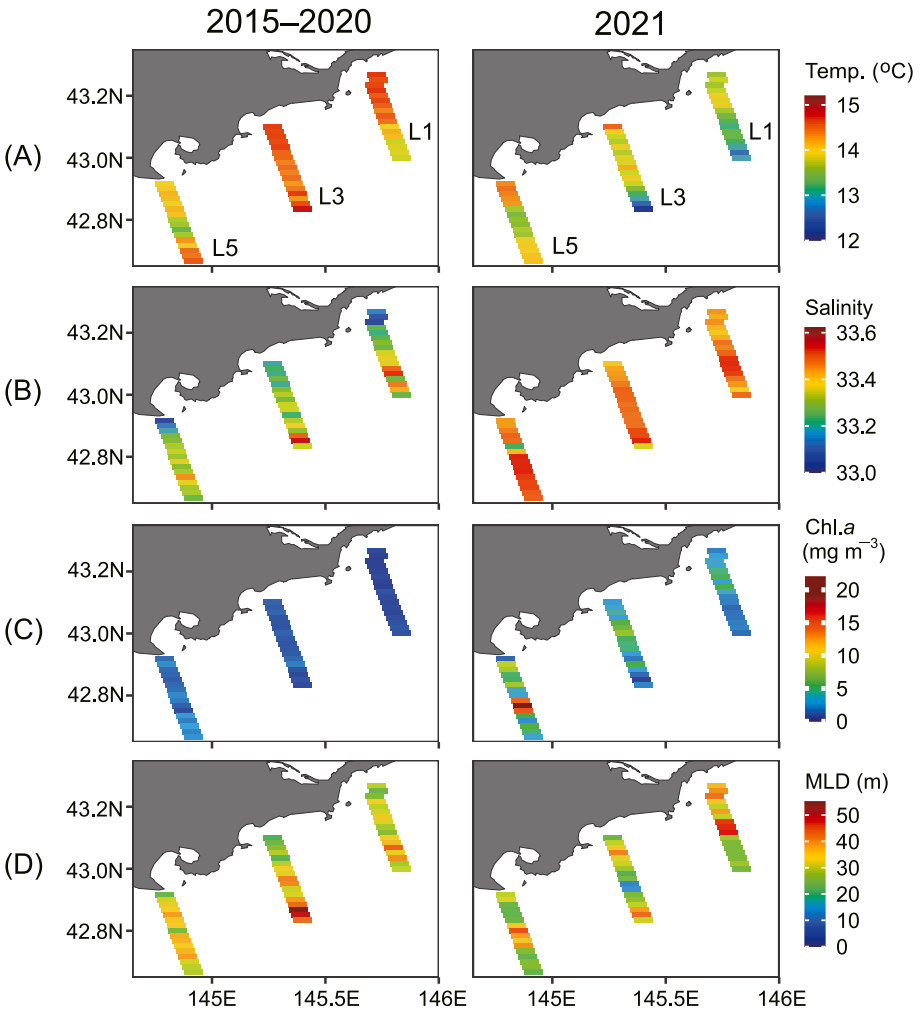

Fig. 3. Distribution of (A) temperature, (B) salinity, (C) chlorophyll-*a* (Chl.*a*) concentrations, and (D) mixed layer depth (MLD) during October. Except for MLD, variables were measured at a depth of 10 m. Left-hand panels show data averaged over October 2015–2020, and right-hand panels show data for October 2021.

periods at 0 and 10 m, despite the significant differences at depths below 20 m (Fig. 9G), and N/Si ratios were not significantly different below 10 m, despite the significant differences observed at 0 m (Fig. 9H). These near-surface patterns suggest that the high abundances of *Karenia* spp. at the sea surface seriously affected the composition of phytoplankton species at shallow depths (Figs. 7 and 8), altered the stoichiometry of nutrient uptake, and caused the balance of nitrate, phosphate, and silicate to diverge from the 2015–2020 averages.

4. Discussion

4.1. Processes in the mixed layer in 2021

Here, we discuss the physico-biochemical processes that occurred in the mixed layer during October 2021 in terms of averages over the observed region (i.e., lines L1, L3, and L5). During that month, the mixed layer was deepening because of seasonal sea surface cooling, and the average mixed layer depth was 31 m (Fig. 6D). The nearly homogenous distribution of nutrients within the mixed layer (Fig. 9D–F) indicates active vertical convection. In contrast, the higher chlorophyll-*a* concentrations at the sea surface suggest that the distributions of *Karenia* spp. were limited to the immediate vicinity of the sea surface. This pattern differed from the subsurface chlorophyll-*a* maximum in other regions (e.g., *Karenia brevis* on the West Florida Shelf; Weisberg et al., 2019). Moreover, this sea surface–intensified structure implies that the movement of *Karenia* spp. was not entirely passive but that *Karenia* spp. moved actively toward the sea surface by, for example, exploiting their positive buoyancy (e.g., Lännergren, 1979) or actively moving (Heil et al., 2014; Hu et al., 2016; Schofield et al., 2006). Diel migration of chlorophyll-*a* concentrations was not detected in our observations, probably because our surveys occurred only between 04:00 to 18:30 JST (Japan Standard Time), and few nighttime surveys were conducted. According to laboratory experiments conducted by Shikata et al. (2014), *Karenia mikimotoi* sink away from the water surface at night and cluster against the water surface during the day when the salinity is vertically homogeneous.

During October 2021, nutrients were being entrained into the mixed layer from deeper waters, which consisted of Modified Soya Warm Current Water with an apparent salinity maximum (Fig. 9B) and had higher nutrient concentrations in 2021 than in 2015–2020 (Fig. 9D–F). The entrained deeper waters, which were associated with lower phytoplankton abundance than the mixed layer (Fig. 9C), had higher N/P and similar N/Si ratios than the average values during 2015–2020 (Fig. 9G and H). The implication is that if phytoplankton had not been present in the mixed layer, N/P and N/Si ratios near the sea surface (i.e., 0–30 m) would have been higher than those observed in 2021. In fact, the high *Karenia* spp. abundance near the sea surface likely drew down nutrient levels, especially nitrate, at shallow depths and created anomalous N/P and N/Si ratios. The anomalous nutrient balance might have been confined to the immediate vicinity of the sea surface because as soon as the nutrients were taken up by *Karenia* spp., nutrient concentrations in the rest of the mixed layer were homogenized by active

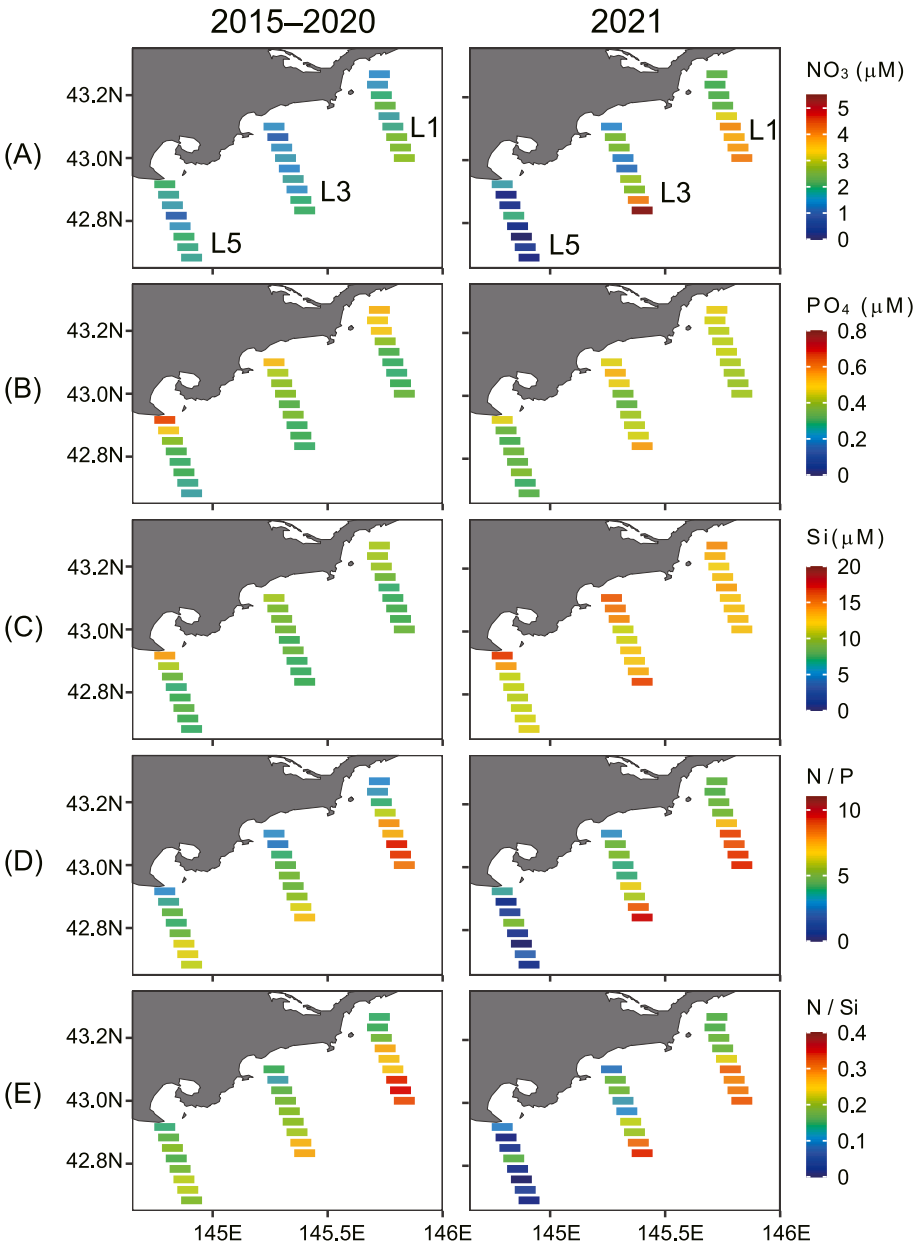

Fig. 4. Same as Fig. 3 but for concentrations of (A) nitrate, (B) phosphate, and (C) silicate and (D) N/P and (E) N/Si ratios at a depth of 10 m.

vertical convection.

Incidentally, it should be noted that the best sampling depth to study *Karenia* spp. during the 2021 HABs was the sea surface rather than the depth of 10 m on which our taxonomic monitoring protocol was based. Our post-2015 monitoring protocol was based on the properties of the dominant non-*Karenia* phytoplankton species (mainly, diatoms) during normal years. It will hence be very desirable to extend that monitoring protocol to the sea surface in the near future (n.b., the protocol is being tested now) to more recisely monitor the behavior of *Karenia* spp.

4.2. Spatial variability of the 2021 HABs

The results shown in Figs. 6–9 and Table 1 are based on spatial averages over lines L1, L3, and L5 because our primary focus was on overall conditions throughout the targeted Pacific shelf. However, there were clearly spatial differences among the lines (Figs. 2–5), particularly L5, where *Karenia* spp. were most abundant. The implication is that the features observed along L5 in 2021 were the most representative of *Karenia* spp. outbreaks on the Pacific shelf. L5 in 2021 had the lowest nitrate concentrations at a depth of 10 m among the three lines (Fig. 4A). Those low nitrate concentrations largely explain the extremely low N/P and N/Si ratios observed along this line (Fig. 4D and E). Those low ratios were associated with much lower abundances of diatoms along L5 than along lines L1 and L3 (Fig. 5A). Average nitrate concentrations along L5 were significantly lower in 2021 than in 2015–2020 ($P = 0.0042$), even though average nitrate concentrations along L1, L3, and L5 combined were not significantly different between the two periods (Fig. 6E). The implication is that phytoplankton composition and nutrient balances were most affected by outbreaks of *Karenia* spp. along L5.

Interestingly, nitrate was relatively replete in 2021 along L1 and L3 (Fig. 4A), and nitrate, phosphate, and silicate concentrations were higher along these two lines in 2021 than in 2015–2020 (Fig. 4B and C). Nevertheless, at some stations along L1 and L3, abundances of diatoms, dinoflagellates, picoeukaryotes, and *Synechococcus* spp. were lower in 2021 than in 2015–2020 (Fig. 5B–D). In addition, although information on the abundance of picoeukaryotes and *Synechococcus* spp. was limited

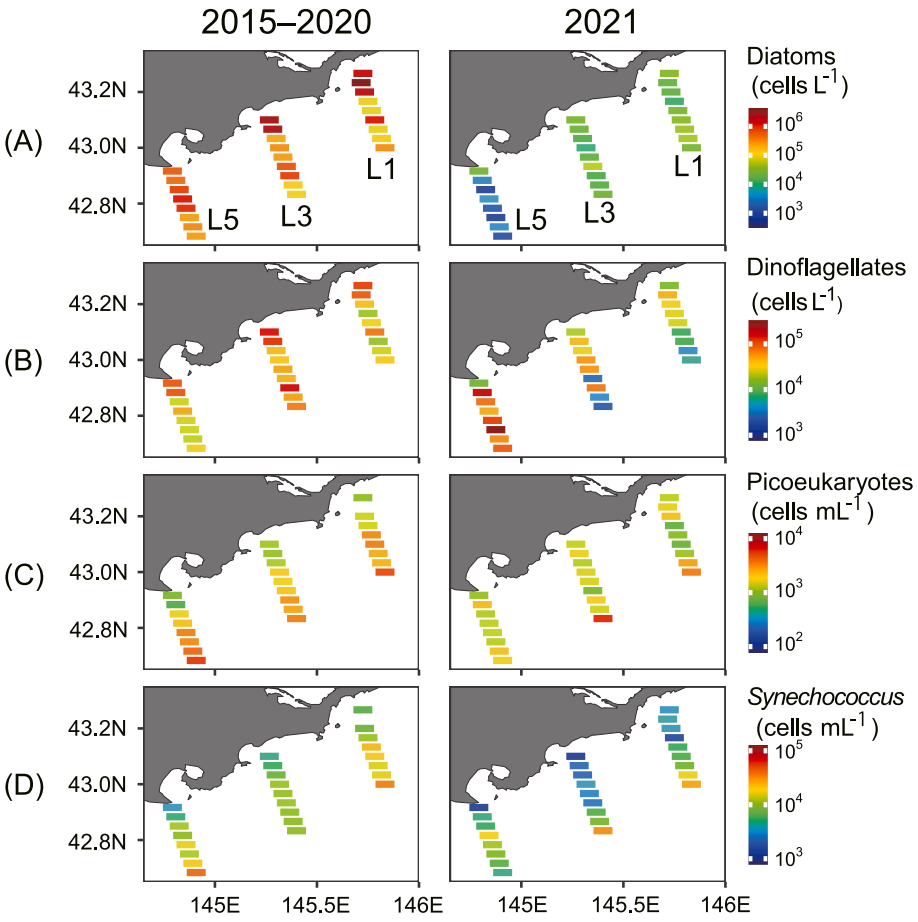

Fig. 5. Same as Fig. 3 but for abundances of (A) diatoms, (B) dinoflagellates, (C) picoeukaryotes, and (D) *Synechococcus* spp. at a depth of 10 m.

to 2020 and 2021 because of missing observations, the above relationships between high nutrient concentrations and lower abundances of picoeukaryotes and *Synechococcus* spp. along L1 and L3 were consistent in comparisons between 2020 and 2021 (Fig. S4). These similarities suggest that the presence of even small numbers of *Karenia* spp. might be sufficient to suppress the growth of many non-*Karenia* algae through allelopathy (Kubanek et al., 2005; Poulin et al., 2018; Poulson-Ellestad et al., 2014; Zheng et al., 2021) as well as interspecific competition for nutrients (Huang et al., 2020; Shen et al., 2022). Because *K. selliformis* and *K. mikimotoi* can be mixotrophic,[2] grazing pressure on picophytoplankton might also explain the reduction of the abundances of picoeukaryotes and *Synechococcus* spp. (Boudriga et al., 2023; Procise, 2012). The role of mixotrophy is important because at present even the most recently developed ecosystem model of *Karenia* blooms (i.e., Takagi et al., 2022) only accounts for interspecific competition for nutrient uptake among *K. selliformis*, diatoms, and non-*Karenia* dinoflagellates. Experimental exposures of non-*Karenia* algae to *K. selliformis* as well as further studies that combine monitoring with modelling are needed to understand the individual and combined effects of allelopathy, mixotrophy, and interspecific competition for nutrients on the Pacific shelf.

4.3. Chlorophyll-*a* cell quota of *Karenia* spp

Chlorophyll-*a* concentrations at a depth of 10 m were ~2.3 times higher in 2021 (mean, 4.398 mg m^{-3}) than in 2015–2020 (mean, 1.954 mg m^{-3}) (Fig. 6C). However, because missing observations biased the enumeration of diatom and dinoflagellate abundances (Figs. S4H and I), we averaged chlorophyll-*a* concentrations at stations where enumeration data were not missing. The mean chlorophyll-*a* concentrations so estimated were 4.475 mg m^{-3} in 2021 and 1.539 mg m^{-3} in 2015–2020 along the L1, L3, and L5 lines at a depth of 10 m. The 2.9-fold increase of chlorophyll-*a* concentrations from 2015–2020 to 2021 corresponded to a 8.8-fold reduction of the sum of the abundances of the 12 categorized taxa—from 579,020 cells L^{-1} in 2015–2020 to 65,857 cells L^{-1} in 2021 (Table 1). The indication was that the cell quotas of chlorophyll-*a* were markedly higher for *Karenia* spp. than for other taxa.

The cell quotas of chlorophyll-*a* for representative species have been reported as follows: 37.0 pg $cell^{-1}$ for *K. selliformis* (Yamaguchi et al., 2022), 6.1–10.1 pg $cell^{-1}$ for *Karenia brevis* (Hardison et al., 2012), 15.4 pg $cell^{-1}$ for *K. mikimotoi* (Chang and Gall, 2013), 0.1–0.37 pg $cell^{-1}$ for *S. costatum* (Speeckaert et al., 2019), ~1 pg $cell^{-1}$ for *L. danicus*, ~2 pg $cell^{-1}$ for *Nitzschia* sp., and ~6–40 pg $cell^{-1}$ for *Thalassiosira* spp. (*Thalassiosira rotula, Thalassiosira hyaline, Thalassiosira guillardi, Thalassiosira nordenskioeldii*) collected in the Oyashio area (Saito and Tsuda, 2003). Briefly, *Karenia* spp. and *Thalassiosira* spp. tend to have relatively high cell quotas of chlorophyll-*a*, although the cell quotas for *Thalassiosira* spp. depend strongly on species.

We estimated the cell quotas of chlorophyll-*a* for *Karenia* spp. to be 39.8, 49.7, 59.7, 69.6, 79.6, 89.5, and 99.5 pg $cell^{-1}$ on the assumption that 40, 50, 60, 70, 80, 90, and 100% of the chlorophyll-*a* concentrations observed in 2021 (i.e., 4.475 mg m^{-3}) were accounted for by *Karenia* spp., respectively. The estimate based on the assumption of 40% was the closest to the estimate for *K. selliformis* (37.0 pg $cell^{-1}$) by Yamaguchi et al. (2022).

How can we explain the other 40% of the observed chlorophyll-*a*

[2] The mixotrophy of *K. selliformis* has not been confirmed and is still controversial (e.g., Ok et al., 2023).

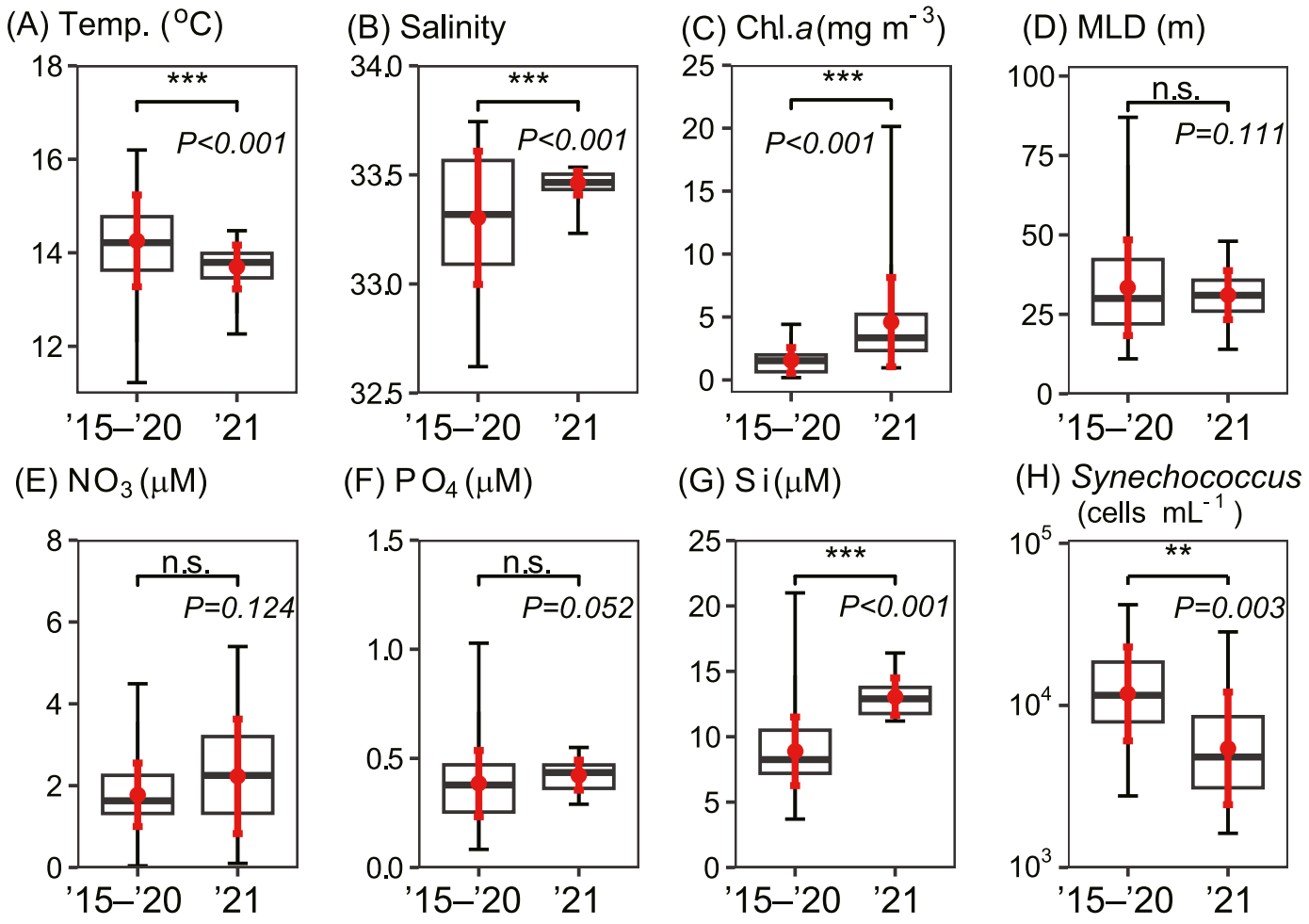

Fig. 6. Comparison of environmental variables at a depth of 10 m along lines L1, L3, and L5 between October 2015–2020 and 2021. (A) Temperature, (B) salinity, (C) chlorophyll-*a* (Chl.*a*) concentration, (D) mixed layer depth (MLD), (E) nitrate, (F) phosphate, (G) silicate concentrations, and (H) *Synechococcus* spp. abundance. Black vertical bars indicate the range; upper, middle, and lower horizontal lines in each box denote the 25th percentile, median, and 75th percentile, respectively; and red circles and vertical bars indicate means and standard deviations, respectively. *P*-values were estimated by Welch's *t*-test. N.S., not significant. The symbols *, **, and *** indicate $0.01 < P \leq 0.05$, $0.001 < P \leq 0.01$, and $P \leq 0.001$, respectively.

Table 1
Abundance (cells L^{-1}) of 12 categorized taxa in October 2015–2020 and 2021. Abundances were measured at a depth of 10 m and were averaged over lines L1, L3, and L5 during the target period.

Species	2015–2020	2021
Dinoflagellates		
Karenia spp.	15	44,992
Gyrodinium spp.	998	993
Ceratium kofoidii	109	270
Gonyaulax spp.	7	148
Scrippsiella spp.	26	187
Other dinoflagellates	345	224
Diatoms		
Lauderia annulata	820	1163
Skeletonema costatum	362,244	4976
Thalassiosira spp.	131,154	9970
Leptocylindrus danicus	13,994	770
Asterionellopsis glacialis	8407	476
Other diatoms	60,901	1688

concentrations? First, there are undoubtedly some errors in the observed chlorophyll-*a* concentrations because those values were estimated from optical sensors (see Fig. S3). For 2021, the root mean squared error of the estimated value was 0.467 mg m^{-3} (Fig. S3), which was 10.4% of the 2021 mean. Second, the chlorophyll-*a* content of 37.0 pg $cell^{-1}$ for *K. selliformis* estimated from the regression between *in situ* chlorophyll-*a* concentrations and *K. selliformis* abundances (Yamaguchi et al., 2022) could include some estimation errors. If the cell quota was underestimated because of such errors, the chlorophyll-*a* concentrations not accounted for by *K. selliformis* (i.e., 2.685 mg m^{-3}) would be reduced. Third, algal taxa other than *Karenia* spp. could have accounted for some of the chlorophyll-*a* concentrations. For example, if *Thalassiosira* spp., which accounted for 15.1% of relative abundance in 2021 (Fig. 8), had a chlorophyll-*a* cell quota of 40.0 pg $cell^{-1}$, they could have accounted for 8.9% (i.e., 0.400 mg m^{-3}) of the 2021 mean. Fourth, our estimation of the chlorophyll-*a* cell quota of *Karenia* spp. might depend strongly on their growth phase. Our tentative culture experiments with *K. selliformis* (not shown) have revealed that the number of burst cells associated with broken/dead cells with active chlorophyll fluorescence (Wang et al., 2021) increases during the decline phase of growth. In our enumeration, such burst cells of *Karenia* spp. were taxonomically eliminated and not counted in the Lugol's samples. If large numbers of burst cells with active chlorophyll fluorescence were present in the collected water sample, some of the other 40% of the observed chlorophyll-*a* concentrations could be accounted for by burst cells. Because cell death and cell lysis (e.g., burst cells) are among the general mechanisms typically postulated for bloom termination (Vargo, 2009), there is a need to

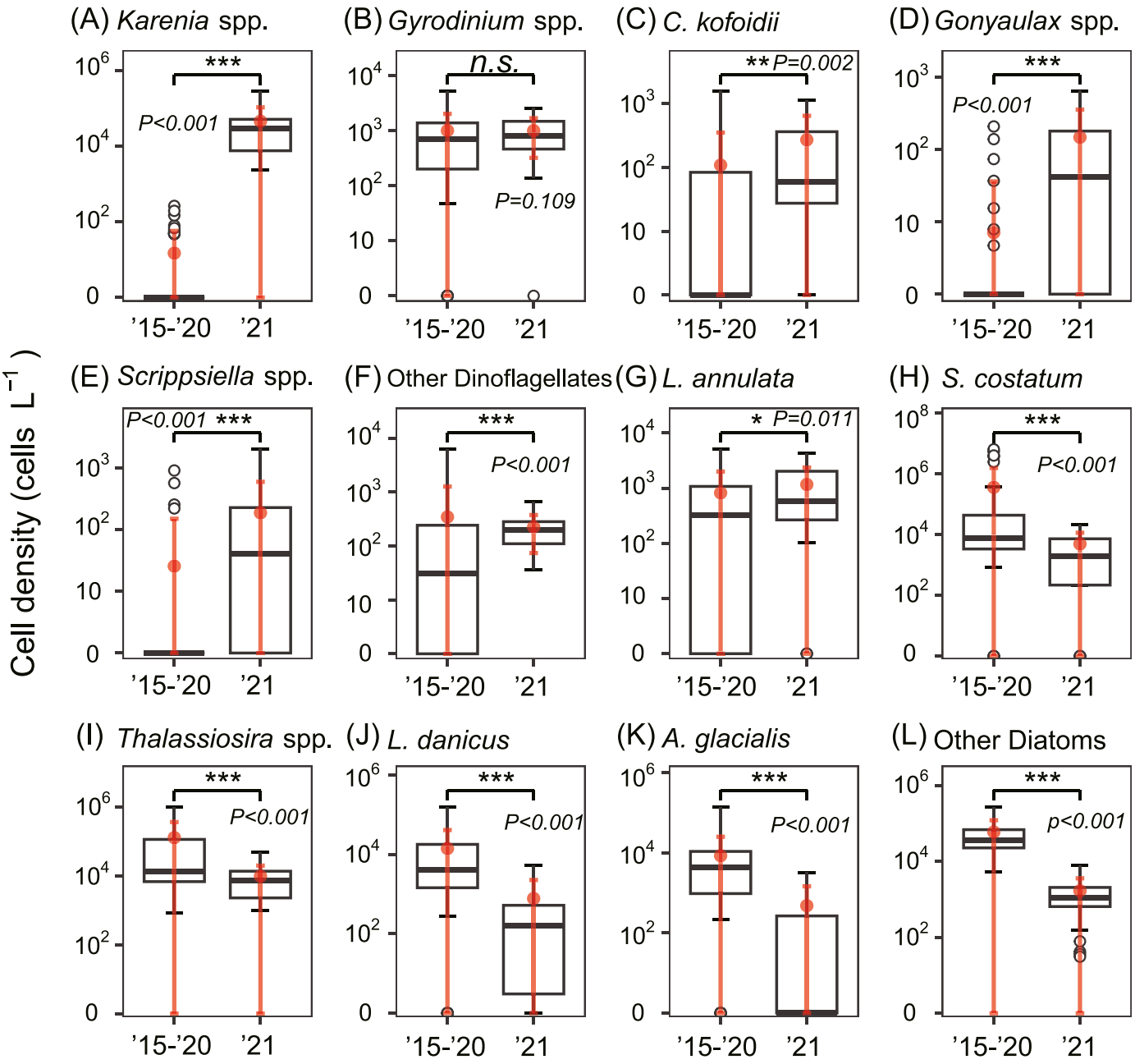

Fig. 7. Same as Fig. 6 but for abundances of (A) *Karenia* spp., (B) *Gyrodinium* spp., (C) *Ceratium kofoidii,* (D) *Gonyaulax* spp., (E) *Scrippsiella* spp., (F) other dinoflagellates, (G) *Lauderia annulata*, (H) *Skeletonema costatum*, (I) *Thalassiosira* spp., (J) *Leptocylindrus danicus*, (K) *Asterionellopsis glacialis*, and (L) other diatoms.

clarify the extent to which burst cells contributed to the *in situ* chlorophyll-*a* concentrations during the 2021 HABs, but such clarification was beyond the scope of our study.

4.4. Comparison to climatology of nutrients around the shelf

Vertical profiles averaged over the Pacific shelf (Fig. 9D–F) show that vertical entrainment supplied higher concentrations of nitrate, phosphate, and silicate to the vicinity of the sea surface in 2021 than in 2015–2020. Kuroda et al. (2021a) have suggested that oceanic nutrients entrained into the vicinity of the sea surface after MHWs by intermittent and seasonal development of the mixed layer (i.e., after mid-August 2021) could have played an important role in the occurrence of the 2021 HABs. However, nutrient concentrations in October 2021 below the depth of the mixed layer (about 30 m on average) at Station A01 on the shelf were within the range of the climatological mean ± one standard deviation, except at depths of 40–50 m (Fig. 10A–C). Nutrient concentrations at Station A02 on the shelf break in 2021 were also comparable to the climatological mean within the surface mixed layer (Fig. 10D–F). Below the mixed layer, nutrient concentrations in 2021 tended to be higher than the climatological mean by one standard deviation. The implication is that the supply of nutrients to sea surface waters on the shelf was somewhat higher during October 2021 than 2015–2020 but never departed greatly from the climatological mean.

5. Conclusions

Unprecedented, large-scale HABs occurred in Pacific coastal shelf waters off the southeastern coast of Hokkaido, Japan, in autumn 2021. By analyzing *in situ* monitoring data in October 2015–2021, we identified how the 2021 HABs changed the structure of the lower-trophic-level ecosystem over the coastal shelf waters impacted by the HABs. Our

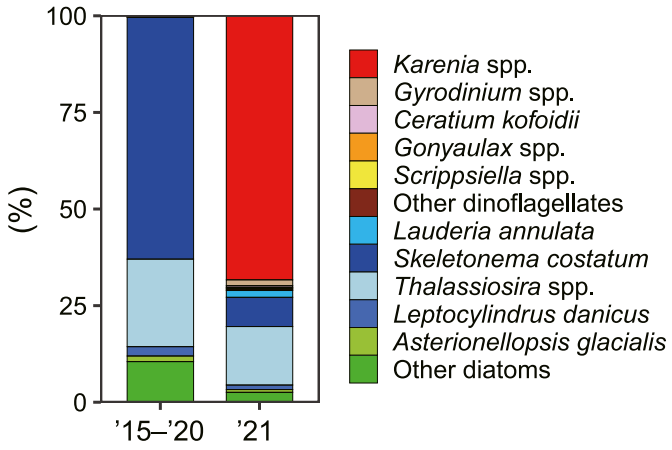

Fig. 8. Percent composition of 12 categorized taxa in 2015–2020 and 2021. Abundances were measured at a depth of 10 m and averaged over lines L1, L3, and L5 during the target period.

results revealed that coastal shelf waters where diatoms were the most dominant phytoplankton (2015–2020) prior to HAB occurrence changed drastically during HAB occurrence to a silicate-replete habitat where *Karenia* spp. was the dominant taxon (2021). Chlorophyll-*a* concentrations at a depth of 10 m were 2.3-fold higher in 2021 than in 2015–2020 and had a clear sea surface–intensified structure. The composition of major phytoplankton taxa was less balanced in 2021. Although the abundance change of dinoflagellates was taxa dependent, surprisingly, the abundance of *Synechococcus* spp. at a depth of 10 m declined in 2021, even at stations where nitrate and phosphate were replete. Further work is needed to identify the extent to which allelopathy and mixotrophy by *K. selliformis* and interspecific competition for nutrients contributed to the changes in phytoplankton composition. Such studies could take the form of biological exposure experiments of non-*Karenia* algae to *K. selliformis* as well as further integrations of monitoring and modelling data.

CRediT authorship contribution statement

Yukiko Taniuchi: Investigation, Data curation, Data analysis, Visualization. Tsuyoshi Watanabe: Taxonomical identification, Data analysis. Tomonori Azumaya, Satomi Takagi, Shigeho Kakehi: Discussion of Karenia modelling, Modification – original draft and revision. Hiromi Kasai: Data curation (nutrients). Takuya Nakanowatari: Investigation, data curation (physical oceanography). Takuya Ohnishi: Investigation. Hiroshi Kuroda: Conceptualization, Writing – original draft and revision.

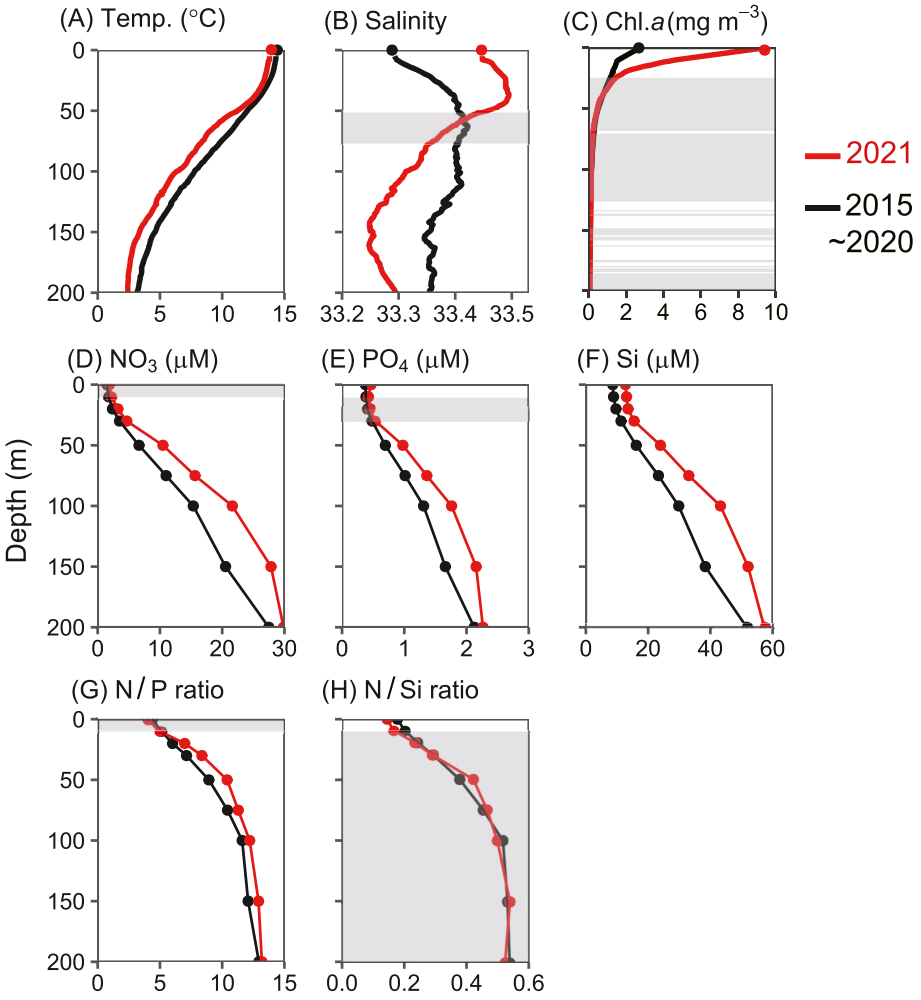

Fig. 9. Vertical profiles averaged over lines L1, L3, and L5 during October 2015–2020 (black lines) and October 2021 (red lines). (A) Temperature, (B) salinity, (C) chlorophyll-*a* (Chl.*a*) concentration, (D) nitrate, (E) phosphate, (F) silicate concentration, (G) N/P ratio, and (H) N/Si ratio. Closed circles indicate variables manually determined from water samples. Grey shading indicates that there were no significant differences among depths as determined by using Welch's *t*-test.

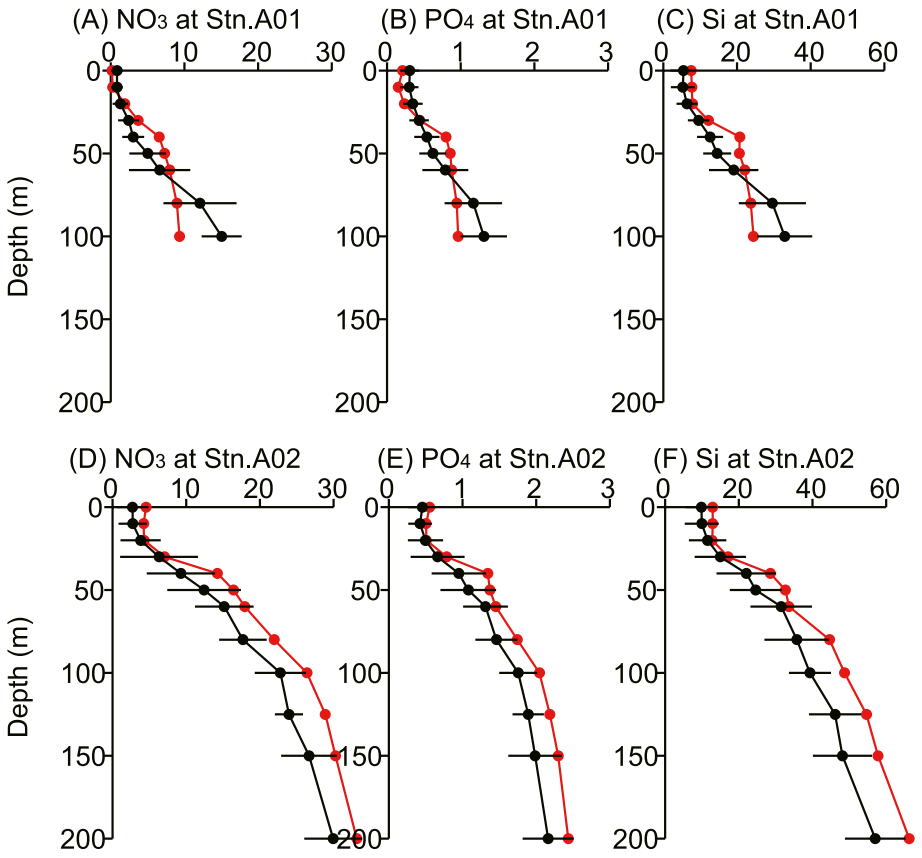

Fig. 10. Vertical profiles of (A) nitrate, (B) phosphate, and (C) silicate concentrations at Station A01, located on the shelf at a water depth of 99 m. (D)–(F) Same as (A)–(C), but for Station A02 near the shelf break at a water depth of 480 m. Red lines correspond to values observed in October 2021. Black lines and horizontal bars indicate the climatological mean and standard deviation, respectively, for October (1993–2011).

Data availability

Data will be made available upon request.

Declaration of competing interest

The authors declare that they have no known competing financial interests or personal relationships that could have appeared to influence the work reported in this paper.

Acknowledgements

We express our deepest gratitude to the captains, officers, and crews of the R/V Hokko-maru for their help during the monitoring of the A and L lines. Thanks are also extended to Dr. K. Kawanobe for preparation of the phytoplankton dataset and to Mss. H. Kunou, K. Chiba, and M. Nakamura for supporting the monitoring and related analyses. This work was funded by the Fisheries Resources Institute of the Japan Fisheries Research and Education Agency (no grant number) and by the Ministry of Education, Culture, Sports, Science and Technology (KAKEN grant 22H05203). In addition, the vessel-monitoring program was supported by the Stock Assessment Program of the Fisheries Research and Education Agency of Japan and Fisheries Agency. However, the content of this study does not necessarily reflect the views of the Fisheries Agency.

Appendix A. Supplementary data

Supplementary data to this article can be found online at https://doi.org/10.1016/j.csr.2023.105114.

References

Bondur, V., Zamshin, V., Chvertkova, O., Matrosova, E., Khodaeva, V., 2021. Detection and analysis of the causes of intensive harmful algal bloom in Kamchatka based on satellite data. J. Mar. Sci. Eng. 9, 1092. https://doi.org/10.3390/jmse9101092.

Boudriga, I., Abdennadher, M., Khammeri, Y., Mahfoudi, M., Quéméneur, M., Hamza, A., Bel haj Hmida, N., Zouari, A.B., Hassen, M.B., 2023. *Karenia selliformis* bloom dynamics and growth rate estimation in the Sfax harbour (Tunisia), by using automated flow cytometry equipped with image in flow, during autumn 2019. Harmful Algae 121, 102366. https://doi.org/10.1016/j.hal.2022.102366.

Chang, F.H., Gall, M., 2013. Pigment compositions and toxic effects of three harmful *Karenia* species, *Karenia concordia, Karenia brevisulcata* and *Karenia mikimotoi* (Gymnodiniales, Dinophyceae), on rotifers and brine shrimps. Harmful Algae 27, 113–120. https://doi.org/10.1016/j.hal.2013.05.005.

Dodson, A.N., Thomas, W.H., 1964. Concentrating plankton in a gentle fashion. Limnol. Oceanogr. 9, 455–456. https://doi.org/10.4319/lo.1964.9.3.0455.

Frölicher, T.L., Laufkötter, C., 2018. Emerging risks from marine heat waves. Nat. Commun. 9, 650. https://doi.org/10.1038/s41467-018-03163-6.

Frölicher, T.L., Fischer, E.M., Gruber, N., 2018. Marine heatwaves under global warming. Nature 560, 360–364. https://doi.org/10.1038/s41586-018-0383-9.

Gobler, C.J., 2020. Climate change and harmful algal blooms: insights and perspective. Harmful Algae 91, 101731. https://doi.org/10.1016/j.hal.2019.101731.

Gobler, C.J., Doherty, O.M., Hattenrath-Lehmann, T.K., Griffith, A.W., Kang, Y., Litaker, R.W., 2017. Ocean warming since 1982 has expanded the niche of toxic algal blooms in the North Atlantic and North Pacific oceans. Proc. Natl. Acad. Sci. USA 114, 4975–4980. https://doi.org/10.1073/pnas.1619575114.

Hasegawa, N., Watanabe, T., Unuma, T., Yokota, T., Izumida, D., Nakagawa, T., Kurokawa, T., Takagi, S., Azumaya, T., Taniuchi, Y., Kuroda, H., Kitatsuji, S., Abe, K., 2022. Repeated reaching of the harmful algal bloom of *Karenia* spp. around the Pacific shoreline of Kushiro, eastern Hokkaido, Japan, during autumn 2021. Fish. Sci. 88, 787–803. https://doi.org/10.1007/s12562-022-01642-w.

Hardison, D.R., Sunda, W.G., Litaker, R.W., Shea, D., Tester, P.A., 2012. Nitrogen limitation increases brevetoxins in *Karenia brevis* (Dinophyceae): implications for bloom toxicity. J. Phycol. 48, 844–858. https://doi.org/10.1111/j.1529-8817.2012.01186.x.

Hasle, G.R., Syvertsen, E.E., 1997. Marine diatoms. In: Tomas, C.R. (Ed.), Identifying Marine Phytoplankton. Academic Press, Inc, San Diego, pp. 5–385.

Heil, C.A., Bronk, D.A., Mulholland, M.R., O'Neil, J.M., Bernhardt, P.W., Murasko, S., Havens, J.A., Vargo, G.A., 2014. Influence of daylight surface aggregation behavior on nutrient cycling during a *Karenia brevis* (Davis) G. Hansen & Ø. Moestrup bloom:

migration to the surface as a nutrient acquisition strategy. Harmful Algae 38, 86–94. https://doi.org/10.1016/j.hal.2014.06.001.
Higashi, H., Nakada, S., 2022. Specificity of ocean current and water mass off the eastern Hokkaido, Japan, in the summer and autumn 2021 when the harmful algal bloom occurred. J. JSCE Ser. B2 (Coastal Engineering) 78,. https://doi.org/10.2208/kaigan.78.2_I_823. I_823–I_828 (in Japanese with English abstract).
Hobday, A.J., Alexander, L.V., Perkins, S.E., Smale, D.A., Straub, S.C., Oliver, E.C.J., Benthuysen, J.A., Burrows, M.T., Donat, M.G., Feng, M., Holbrook, N.J., Moore, P.J., Scannell, H.A., Gupta, A.S., Wernberg, T., 2016. A hierarchical approach to defining marine heatwaves. Prog. Oceanogr. 141, 227–238. https://doi.org/10.1016/j.pocean.2015.12.014.
Hu, C., Barnes, B.B., Qi, L., Lembke, C., English, D., 2016. Vertical migration of *Karenia brevis* in the northeastern Gulf of Mexico observed from glider measurements. Harmful Algae 58, 59–65. https://doi.org/10.1016/j.hal.2016.07.005.
Huang, K., Feng, Q., Zhang, Y., Ou, L., Cen, J., Lu, S., Qi, Y., 2020. Comparative uptake and assimilation of nitrate, ammonium, and urea by dinoflagellate *Karenia mikimotoi* and diatom *Skeletonema costatum* s.l. in the coastal waters of the East China Sea. Mar. Pollut. Bull. 155, 111200 https://doi.org/10.1016/j.marpolbul.2020.111200.
IPCC [Intergovernmental Panel on Climate Change], 2019. IPCC Special Report on the Ocean and Cryosphere in a Changing Climate. IPCC, Geneva, Switzerland. Available online at: https://www.ipcc.ch/srocc. (Accessed 24 January 2023).
Iwataki, M., Lum, W.M., Kuwata, K., Takahashi, K., Arima, D., Kuribayashi, T., Kosaka, Y., Hasegawa, N., Watanabe, T., Shikata, T., Isada, T., Orlova, T.Y., Sakamoto, S., 2022. Morphological variation and phylogeny of *Karenia selliformis* (Gymnodiniales, Dinophyceae) in an intensive cold-water algal bloom in eastern Hokkaido, Japan in September–November 2021. Harmful Algae 114, 102204. https://doi.org/10.1016/j.hal.2022.102204.
Kasai, H., Saito, H., Tsuda, A., 1998. Estimation of standing stock of chlorophyll a and primary production from remote-sensed ocean color in the Oyashio region, the western subarctic Pacific, during the spring bloom in 1997. J. Oceanogr. 54, 527–537. https://doi.org/10.1007/BF02742454.
Kubanek, J., Hicks, M.K., Naar, J., Villareal, T.A., 2005. Does the red tide dinoflagellate *Karenia brevis* use allelopathy to outcompete other phytoplankton? Limnol. Oceanogr. 3 https://doi.org/10.4319/lo.2005.50.3.0883.
Kuroda, H., Wagawa, T., Kakehi, S., Shimizu, Y., Kusaka, A., Okunishi, T., Hasegawa, D., Ito, S., 2017. Long-term mean and seasonal variation of altimetry-derived Oyashio transport across the A-line off the southeastern coast of Hokkaido, Japan. Deep-Sea Res. I 121, 95–109. https://doi.org/10.1016/j.dsr.2016.12.006.
Kuroda, H., Toya, Y., 2020. High-resolution sea surface temperatures derived from Landsat 8: a study of submesoscale frontal structures on the Pacific shelf off the Hokkaido coast, Japan. Rem. Sens. 12, 3326. https://doi.org/10.3390/rs12203326.
Kuroda, H., Setou, T., 2021. Extensive marine heatwaves at the sea surface in the northwestern Pacific Ocean in summer 2021. Rem. Sens. 13, 3989. https://doi.org/10.3390/rs13193989.
Kuroda, H., Azumaya, T., Setou, T., Hasegawa, N., 2021a. Unprecedented outbreak of harmful algae in Pacific coastal waters off southeast Hokkaido, Japan, during late summer 2021 after record-breaking marine heatwaves. J. Mar. Sci. Eng. 9, 1335. https://doi.org/10.3390/jmse9121335.
Kuroda, H., Suyama, S., Miyamoto, H., Setou, T., Nakanowatari, T., 2021b. Interdecadal variability of the Western Subarctic Gyre in the North Pacific ocean. Deep-Sea Res. Part I 169, 103461. https://doi.org/10.1016/j.dsr.2020.103461.
Kuroda, H., Taniuchi, Y., Kasai, H., Nakanowatari, T., Setou, T., 2021c. Co-occurrence of marine extremes induced by tropical storms and an ocean eddy in summer 2016: anomalous hydrographic conditions in the Pacific shelf waters off southeast Hokkaido, Japan. Atmosphere 12, 888. https://doi.org/10.3390/atmos12070888.
Kuroda, H., Taniuchi, Y., Watanabe, T., Azumaya, T., Hasegawa, N., 2022. Distribution of harmful algae (*Karenia* spp.) in October 2021 off southeast Hokkaido, Japan. Front. Mar. Sci. 9, 841364 https://doi.org/10.3389/fmars.2022.841364.
Kusaka, A., Azumaya, T., Kawasaki, Y., 2013. Monthly variations of hydrographic structures and water mass distribution off the Doto area. Japan. J. Oceanogr. 69, 295–312. https://doi.org/10.1007/s10872-013-0174-8.
Lännergren, C., 1979. Buoyancy of natural populations of marine phytoplankton. Mar. Biol. 54, 1–10. https://doi.org/10.1007/BF00387045.
Lefebvre, K.A., Quakenbush, L., Frame, E., Huntington, K.B., Sheffield, G., Stimmelmayr, R., Bryan, A., Kendrick, P., Ziel, H., Goldstein, T., Snyder, J.A., Gelatt, T., Gulland, F., Dickerson, B., Gill, V., 2016. Prevalence of algal toxins in Alaskan marine mammals foraging in a changing arctic and subarctic environment. Harmful Algae 55, 13–24. https://doi.org/10.1016/j.hal.2016.01.007.
McCabe, R.M., Hickey, B.M., Kudela, R.M., Lefebvre, K.A., Adams, N.G., Bill, B.D., Gulland, F.M.D., Thomson, R.E., Cochlan, W.P., Trainer, V.L., 2016. An unprecedented coastwide toxic algal bloom linked to anomalous ocean conditions. Geophys. Res. Lett. 43, 10366–10376. https://doi.org/10.1002/2016GL070023.
Oguma, S., Ono, T., Kusaka, A., Kasai, H., Kawasaki, Y., Azumaya, T., 2008. Isotopic tracers for water masses in the coastal region of eastern Hokkaido. J. Oceanogr. 54, 525–539. https://doi.org/10.1007/s10872-008-0044-y.
Ok, J.H., Jeong, H.J., Lim, A.S., Kang, H.C., You, J.H., Park, S.A., Eom, S.H., 2023. Lack of mixotrophy in three *Karenia* species and the prey spectrum of *Karenia mikimotoi* (Gymnodiniales, Dinophyceae). ALGAE 38, 39–55. https://doi.org/10.4490/algae.2023.38.2.28.
Oliver, E.C.J., Donat, M.G., Burrows, M.T., Moore, P.J., Smale, D.A., Alexander, L.V., Benthuysen, J.A., Feng, M., Gupta, A.S., Hobday, A.J., Holbrook, N.J., Perkins-Kirkpatrick, S.E., Scannell, H.A., Staub, S.C., Wernberg, T., 2018. Longer and more frequent marine heatwaves over the past century. Nat. Commun. 9, 1324. https://doi.org/10.1038/s41467-018-03732-9.
Oliver, E.C.J., Burrows, M.T., Donat, M.G., Sen-Gupta, A., Alexander, L.V., Perkins-Kirkpatrick, S.E., Benthuysen, J.A., Hobday, A.J., Holbrook, N.J., Moore, P.J., Thomsen, M.S., Wernberg, T., Smale, D.A., 2019. Projected marine heatwaves in the 21st Century and the potential for ecological impact. Front. Mar. Sci. 6, 734. https://doi.org/10.3389/fmars.2019.00734.
Oliver, E.C.J., Benthuysen, J.A., Darmaraki, S., Donat, M.G., Hobday, A.J., Holbrook, N.J., Schlegel, R.W., Sen-Gupta, A., 2021. Marine heatwaves. Ann. Rev. Mar. Sci 13, 313–342. https://doi.org/10.1146/annurev-marine-032720-095144.
Orlova, T.Y., Aleksanin, A.I., Lepskaya, E.V., Efimova, K.V., Selina, M.S., Morozova, T.V., Stonik, I.V., Kachur, V.A., Karpenko, A.A., Vinnikov, K.A., Adrianov, A.V., Iwataki, M., 2022. A massive bloom of *Karenia* species (Dinophyceae) off the Kamchatka coast, Russia, in the fall of 2020. Harmful Algae 120, 102337. https://doi.org/10.1016/j.hal.2022.102337.
Poulin, R.X., Hogan, S., Poulson-Ellestad, K.L., Brown, E., Fernandez, F.M., Kubanek, J., 2018. *Karenia brevis* allelopathy compromises the lipidome, membrane integrity, and photosynthesis of competitors. Sci. Rep. 8, 9572. https://doi.org/10.1038/s41598-018-27845-9.
Poulson-Ellestad, K., Mcmillan, E., Montoya, J.P., Kubanek, J., 2014. Are offshore phytoplankton susceptible to *Karenia brevis* allelopathy? J. Plankton Res. 36, 1344–1356. https://doi.org/10.1093/plankt/fbu064.
Procise, L.A., 2012. Grazing on *Synechococcus* Spp. By the Red-Tide Dinoflagellate *Karenia Brevis*: Implications for Bloom Dynamics in the Gulf of Mexico. Doctor of Philosophy (PhD), Dissertation, Ocean & Earth Sciences. Old Dominion University. https://doi.org/10.25777/jy09-7349. https://digitalcommons.odu.edu/oeas_etds/59.
Roberts, S.D., Van Ruth, P.D., Wilkinson, C., Bastianello, S.S., Bansemer, M.S., 2019. Marine heatwave, harmful algae blooms and an extensive fish kill event during 2013 in south Australia. Front. Mar. Sci. 6, 610. https://doi.org/10.3389/fmars.2019.00610.
Ryan, J.P., Kudela, R.M., Birch, J.M., Blum, M., Bowers, H.A., Chavez, F.P., Doucette, G. J., Hayashi, K., Marin-III, R., Mikulski, C.M., Pennington, J.T., Scholin, C.A., Smith, G.J., Woods, A., Zhang, Y., 2017. Causality of an extreme harmful algal bloom in Monterey Bay, California, during the 2014–2016 northeast Pacific warm anomaly. Geophys. Res. Lett. 44, 5571–5579. https://doi.org/10.1002/2017GL072637.
Saito, H., Kasai, H., Kashiwai, M., Kawasaki, Y., Kono, T., Taguchi, S., Tsuda, A., 1998. General description of seasonal variations in nutrients, chlorophyll a, and netplankton biomass along the A-line transect, western subarctic Pacific, from 1990 to 1994. Bull. Hokkaido Natl. Fish. Res. Inst. 62, 1–62.
Saito, H., Tsuda, A., 2003. Influence of light intensity on diatom physiology and nutrient dynamics in the Oyashio region. Prog. Oceanogr. 57, 251–263. https://doi.org/10.1016/S0079-6611(03)00100-9.
Sakurai, Y., 2007. An overview of the Oyashio ecosystem. Deep-Sea Res. II 54, 2526–2542. https://doi.org/10.1016/j.dsr2.2007.02.007.
Schofield, O., Kerfoot, J., Mahoney, K., Moline, M., Oliver, M., Lohrenz, S., Kirkpatrick, G., 2006. Vertical migration of the toxic dinoflagellate *Karenia brevis* and the impact on ocean optical properties. J. Geophys. Res. 111, C06009 https://doi.org/10.1029/2005JC003115.
Shen, A., Liu, H., Xin, Q., Hu, Q., Wang, X., Chen, J., 2022. Responses of marine diatom–dinoflagellate interspecific competition to different phosphorus sources. J. Mar. Sci. Eng. 10, 1972. https://doi.org/10.3390/jmse10121972.
Shikata, T., Sakamoto, S., Onitsuka, G., Aoki, K., Yamaguchi, M., 2014. Effects of salinity on diel vertical migration behavior in two red-tide algae, *Chattonella antiqua* and *Karenia mikimotoi*. Plankton Benthos Res. 9, 42–50.
Smith, K.E., Burrows, M.T., Hobday, A.J., Sen-Gupta, A., Moore, P.J., Thomsen, M., Wernberg, T., Smale, D.A., 2021. Socioeconomic impacts of marine heatwaves: global issues and opportunities. Science 374, eabj3593. https://doi.org/10.1126/science.abj3593.
Speeckaert, G., Borges, A.V., Gypens, N., 2019. Salinity and growth effects on dimethylsulfoniopropionate (DMSP) and dimethylsulfoxide (DMSO) cell quotas of *Skeletonema costatum, Phaeocystis globosa* and *Heterocapsa triquetra*. Estuar. Coast. Shelf Sci. 226, 106275 https://doi.org/10.1016/j.ecss.2019.106275.
Strickland, J.D.H., Parsons, T.R., 1972. A practical handbook of seawater analysis. In: Fisheries Research Board of Canada Bulletin 157, 2nd Edition, p. 310.
Suzuki, R., Ishimaru, T., 1990. An improved method for the determination of phytoplankton chlorophyll using N, N-dimethylformamide. J. Oceanogr. Soc. Jpn. 46, 190–194. https://doi.org/10.1007/BF02125580.
Suzuki, K., Hinuma, A., Saito, H., Kiyosawa, H., Liu, H., Saino, T., Tsuda, A., 2005. Responses of phytoplankton and heterotrophic bacteria in the northwest subarctic Pacific to in situ iron fertilization as estimated by HPLC pigment analysis and flow cytometry. Prog. Oceanogr. 64, 167–187. https://doi.org/10.1016/j.pocean.2005.02.007.
Takagi, S., Kuroda, H., Hasegawa, N., Watanabe, T., Unuma, T., Taniuchi, Y., Yokota, T., Izumida, D., Nakagawa, T., Kurokawa, T., Azumaya, T., 2022. Controlling factors of large-scale harmful algal blooms with *Karenia selliformis* after record-breaking marine heatwaves. Front. Mar. Sci. 9, 939393 https://doi.org/10.3389/fmars.2022.939393.
Trainer, V.L., Moore, S.K., Hallegraeff, G., Kudela, R.M., Clement, A., Mardones, J.I., Cochlan, W., 2019. Pelagic harmful algal blooms and climate change: lessons from nature's experiments with extremes. Harmful Algae 91, 101591. https://doi.org/10.1016/j.hal.2019.03.009.
Vargo, G.A., 2009. A brief summary of the physiology and ecology of Karenia brevis Davis (G. Hansen and Moestrup comb. nov.) red tides on the West Florida Shelf and of hypotheses posed for their initiation, growth, maintenance, and termination. Harmful Algae 8, 573–584. https://doi.org/10.1016/j.hal.2008.11.002.
Wang, W., Liao, P., Li, G., Chen, H., Cen, J., Lu, S., Wong, P.K., An, T., 2021. Photocatalytic inactivation and destruction of harmful microalgae *Karenia mikimotoi* under visible-light irradiation: insights into physiological response and toxicity

assessment. Environ. Res. 198, 111295 https://doi.org/10.1016/j.envres.2021.111295.
Weisberg, R.H., Liu, Y., Lembke, C., Hu, C., Hubbard, K., Garrett, M., 2019. The coastal ocean circulation influence on the 2018 West Florida Shelf *K. brevis* red tide bloom. J. Geophys. Res. Oceans 124, 2501–2512. https://doi.org/10.1029/2018JC014887.
Wells, M.L., Trainer, V.L., Smayda, T.J., Karlson, B.S.O., Trick, C.G., Kudela, R.M., Ishikawa, A., Bernard, S., Wulff, A., Anderson, D.M., Cochlan, E.P., 2015. Harmful algal blooms and climate change: learning from the past and present to forecast the future. Harmful Algae 49, 68–93. https://doi.org/10.1016/j.hal.2015.07.009.
Wells, M.L., Karlson, B., Wulff, A., Kudela, R., Trick, C., Asnaghi, V., Berdalet, E., Cochlan, W., Davidson, K., Rijcke, M.D., Dutkiewicz, S., Hallegraeff, G., Flynn, K.J., Legrand, C., Paerl, H., Silke, J., Suikkanen, S., Thompson, P., Trainer, V.L., 2020. Future HAB science: directions and challenges in a changing climate. Harmful Algae 91, 101632. https://doi.org/10.1016/j.hal.2019.101632.
Yamaguchi, A., Hamao, Y., Matsuno, K., Iida, T., 2022. Horizontal distribution of harmful red-tide *Karenia selliformis* and phytoplankton community along the Pacific coast of Hokkaido in autumn 2021. Bull. Jpn. Soc. Fish. Oceanogr. 86, 41–49. https://doi.org/10.34423/jsfo.86.2_41 (in Japanese with English abstract).
Zheng, J.-W., Mao, X.-T., Ye, M.-H., Li, H.-Y., Liu, J.-S., Yang, W.-D., 2021. Allelopathy and underlying mechanism of *Karenia mikimotoi* on the diatom *Thalassiosira pseudonana* under laboratory condition. Algal Res. 54 https://doi.org/10.1016/j.algal.2021.102229.